COMPUTATIONAL ANALYSIS OF MHD NANOFLUID FLOW ACROSS A HEATED SQUARE CYLINDER WITH HEAT TRANSFER AND ENTROPY GENERATION

Madhu SHARMA*, Bhupendra K. SHARMA, Chandan KUMAWAT***, Arun K. JALAN****, Neyara RADWAN*****

*Department of Bioscience, CASH, Mody University of Science & Technology, Lakshmangarh, Rajasthan, India
**Department of Mathematics, Birla Institute of Technology and Science, Pilani, Rajasthan, India
***School of Computer Science and Artificial Intelligence, SR University, Warangal, Telangana, India
****Department of Mechanical Engineering, Birla Institute of Technology and Science, Pilani, Rajasthan, India
*****Industrial Engineering Department, College of Applied Sciences, AL MAAREFA UNIVERSITY, Riyadh, Saudi Arabia
*****Mechanical Department, Faculty of Engineering, Suez Canal University, El Salam District, Egypt

madhusharma5dec@gmail.com, bhupen_1402@yahoo.co.in, Chandankumawat000@gmail.com, arunjalan@pilani.bits-pilani.ac.in

received 22 September 2023, revised 07 December 2023, accepted 28 December 2023

Abstract: The mixed convection heat transfer of nanofluid flow in a heated square cylinder under the influence of a magnetic field is considered in this paper. ANSYS FLUENT computational fluid dynamics (CFD) software with a finite volume approach is used to solve unsteady two-dimensional Navier-Stokes and energy equations. The numerical solutions for velocity, thermal conductivity, temperature, Nusselt number and the effect of the parameters have been obtained; the intensity of the magnetic field, Richardson number, nanoparticle volume fraction, magnetic field parameter and nanoparticle diameter have also been investigated. The results indicate that as the dimensions of nanoparticles decrease, there is an observed augmentation in heat transfer rates from the square cylinder for a fixed volume concentration. This increment in heat transfer rate becomes approximately 2.5%–5% when nanoparticle size decreases from 100 nm to 30 nm for various particle volume fractions. Moreover, the magnitude of the Nusselt number enhances with the increase in magnetic field intensity and has the opposite impact on the Richardson number. The findings of the present study bear substantial implications for diverse applications, particularly in the realm of thermal management systems, where optimising heat transfer is crucial for enhancing the efficiency of electronic devices, cooling systems and other technological advancements.

Key words: CuO–Water nanofluid, MHD, heated square cylinder, heat transfer, entropy generation

1. INTRODUCTION

Liquid suspensions with nanometer-sized particles are known as nanofluids. Nanofluids are typically made up of nanoparticles ranging in size from 1 nm to 100 nm dispersed in a standard liquid such as water [1, 2], ethylene glycol [3], methanol [4] or blood [5]. The nanofluid can be used to improve the thermal properties of base fluids such as propylene glycol, ethylene glycol, water and oil, among others. They could be used in biomedical and engineering applications such as process industries, cooling, cancer therapy and a variety of others. X-rays, computers, vehicle engines, nuclear reactors, radiators and solar energy could all benefit from nanofluids. Wen and Ding [6] looked at the convective heat transfer properties of an Al2O3-water nanofluid in a copper tube and discovered that increasing the Reynolds number and volumetric ratio of particles improved the heat transfer coefficient. Shahi et al. [7] explored the laminar convective heat transfer of CuO–water nanofluid moving through a square cavity in a laminar flow regime. Bovand et al. [8] showed the effects of Al2O3 – water nanofluid on fluid flow and heat transfer around an equilateral triangle obstacle with varying orientations. Hayat et al. [9] investigated the flow of carbon water nanomaterials with coupled melting heat transfer and thermal radiation effects. The estimated findings revealed that the side-facing flow has the greatest influence of nanoparticles on heat transfer rate enhancement, while the vertex-facing flow has the least. Hayat et al. [10] studied hydromagnetic tangent-hyperbolic fluid flow with varied characteristics and nanoparticles. Natural convection of a nanofluid in the presence of an electric field has recently been studied electrohydrodynamically (EHD). Sheikholeslami and Ellahi [11] investigated the hydrothermal treatment of Fe3O4-ethylene glycol nanofluid in a lid-driven chamber with a sinusoidal upper wall exposed to a non-uniform electric field. Sheikholeslami and Chamkha [12] investigated the heat transmission properties of electrohydrodynamic free convection of a Fe3O4-ethylene glycol nanofluid in a semi-annulus enclosure with a sinusoidal wall in a following investigation. The influence of a magnetic field on Fe3O4-plasma nanofluid flow in a vessel as a targeted medication delivery method was examined by Kandelousi and Ellahi [13]. It was discovered that the existence of a magnetic field had a significant impact on the flow field, and that increasing the Reynolds number and magnetic number reduced the skin friction coefficient. To enhance the energy transportation into fluid flow, Sarfarz et al. [14–15], introduced the ternary hybrid nanofluids over different surfaces such as inclined porous and spiraling disks. In these, they mixed the three different nanoparticles with the base fluid water and stated that, with introducing ternary hybrid nanoparticles, the energy storage is enhanced significantly. Flow behaviour under the effect of MHD through various geometries has been studied in a variety of cases, such as laminar mixed convection flow from a vertical surface with induced magnetic field studied by Chaudhary and Sharma

[16], analysis of heat and mass transfer for a non-Darcian porous medium [17], temperature-dependent viscosity and thermal conductivity analysis studied by Kumawat [18], and mixed convection flow through rotating channel under the presence of inclined magnetic field and joule effect discussed by Mishra and Sharma [19].

Flow past a heated or cooled square cross-section cylinder has drawn a lot of interest over the years. Such research has been motivated by its fundamental nature as well as its relevance in a wide range of engineering applications, including electronic component cooling, compact heat exchangers, combustion chambers in chemical processes, flow dividers in polymer processing applications and energy systems. Crystal growth, high-performance building insulations, multi-shield structures used in nuclear reactors, solar power collectors, food processing, float glass manufacturing, furnaces, drying technologies and other applications use mixed convection flow and heat transmission in a heated square cylinder. Due to their use, numerous writers (Sharma et al. [20], Turki et al. [21], Bouaziz et al. [22] and Hayat et al. [23]) have studied convective heat fluxes inside cavities such as triangular, trapezoidal, cylindrical, wavy, square and so on. Recently, Sharma has discussed the study of heat and mass transfer under the presence of different types of nanoparticles for the different base fluids on the various geometries with different circumstances such as Darcy-Forchheimer hybrid nanofluid flow over the rotating Riga disk using an artificial neural network approach [24], response surface optimisation discussion for the electromagnetohydrodynamic Cu-polyvinyl alcohol/water Jeffrey nanofluid [25], Bayesian regularisation networks approach for the micropolar ternary hybrid nanofluid flow of blood on the curved stretching sheet [26], Arrhenius activation energy determination for gyrotactic microorganism flows over the porous inclined stretching sheet [27].

The knowledge of thermodynamics for fluid circulation in confined regions is based on the fundamental idea of entropy generation, which measures the level of disorder within a system. The afore-mentioned principle exhibits a wide range of applications across several areas associated with thermodynamics. These fields encompass electronic systems, information systems, power collecting systems, and geothermal power plants. Dogonchi et al. [28] performed a mathematical analysis of the entropy generation on buoyancy-driven flow of Fe_3O_4– H_2O nanofluid through two square cylinders under the porous enclosure condition. They used the Finite element approach to find the graphical profile of entropy and velocity in this analysis. Furthermore, they [29] extended their analysis to estimate the entropy generation profile for a porous cavity containing a base fluid mixed with nano-encapsulated phase change materials (NEPCMs) in the presence of an external heat source/sink. According to this study, the presence of the Rayleigh number has a positive impact on the entropy profile. Recently, the study of entropy analysis on water-mixed nanofluid under different fluid flow mediums with different nanoparticles performed by various researchers such as TiO2-water nanofluid through inclined U-shaped domain with non-Newtonian fluid properties [30], non-Newtonian NEPCM inside the inclined chamber under presence of heater [31], Al_2O_3 -water nanofluid flows through a hexagonal-shaped geometry with a periodic magnetic field [32], and for both Newtonian and non-Newtonian models of bio-fluid through curved vessels under different types of stenosis conditions and nanofluids [33–35].

The depth analysis of the existing literature, it is evident that there is a conspicuous absence of experimental or numerical investigations pertaining to mixed convection heat transfer of nanofluids within a heated square cylinder subjected to the influence of a magnetic field. Therefore, this study presents the computational examination of CuO–water nanofluid impact on the heat transfer profile for a heated square cylinder with a magnetic field. The entropy generation also calculates different magnetic field intensities for various nanoparticle volume fractions. The introduction of nanoparticles into the fluid introduces alterations in its thermo-physical properties, thereby engendering intricate interactions among inertia, viscosity and buoyancy forces. This complexity renders the analysis of mixed convection in nanofluids a formidable task. In this work, the impact of several parameters such as nanoparticle volume fraction, nanoparticle size, magnetic field intensity, Richardson number on the velocity, thermal conductivity, Nusselt number and entropy profile have been discussed with the help of both graphs and contours.

Beyond its intrinsic scientific value, this research contributes practical insights with implications for a spectrum of contemporary applications. By providing information on heat exchange enhancement, the study addresses a pressing need for improved thermal management systems. The findings are poised to influence the design and optimisation of various technological applications, spanning electronic devices, cooling systems and other engineering domains where efficient heat transfer is paramount. Thus, the research not only expands the current scientific understanding but also directly informs and advances technology with real-world applications.

1.1. Formulation of the problem

Consider a single-phase approach for nanofluids [36, 37], where the base fluid and nanoparticles are properly blended and may thus be treated as a homogenous mixture. In addition, due to the ultra-fine and low volume fraction of the solid particles, the fluid phase and solid particles are considered to be in thermal equilibrium and travel at the same local velocity. The flow in a vertical plane channel with a built-in heated square cylinder is the system of interest in this scenario. Fig. 1 shows the computational domain and coordinate system for the setup considered in this investigation. In the channel axis, the square cylinder is symmetrically placed. With a uniform free-stream velocity of u_0 and a constant temperature of T_C at the inlet, fluid moving from bottom to top approaches the square cylinder of side h. The temperature of the square cylinder is kept constant. The square cylinder's bottom face is at a distance of X_u = 10 from the channel inlet. X_d = 15 is the distance between the body and the channel outlet. Except for the body force element in the momentum equation, all thermo-physical parameters (e.g. heat capacity and thermal conductivity) are considered to be temperature-independent in this study (Boussinesq approximation). The time-dependent, two-dimensional Navier Stokes and energy equations of incompressible nanofluid are the conservation equations that describe laminar flow and heat transport. The governing equations for nanofluid flow and heat transfer can be stated as follows using the Boussinesq approximation [38, 39]:

$$\frac{\partial u}{\partial x} + \frac{\partial v}{\partial y} = 0 \tag{1}$$

$$\rho_{nf}\left(\frac{\partial u}{\partial t} + u\frac{\partial u}{\partial x} + v\frac{\partial u}{\partial y}\right) = -\frac{\partial p}{\partial x} + \mu_{nf}\left(\frac{\partial^2 u}{\partial x^2} + \frac{\partial^2 u}{\partial y^2}\right) + \mu_0 M\frac{\partial \bar{H}}{\partial x} - \sigma_{nf}B_y^2 u + \sigma_{nf}B_x B_y v, \tag{2}$$

$$\rho_{nf}\left(\frac{\partial v}{\partial t}+u\frac{\partial v}{\partial x}+v\frac{\partial v}{\partial y}\right)=-\frac{\partial p}{\partial y}+\mu_{nf}\left(\frac{\partial^2 v}{\partial x^2}+\frac{\partial^2 v}{\partial y^2}\right)+\mu_0 M\frac{\partial \bar{H}}{\partial y}-\sigma_{nf}B_x^2 v+\sigma_{nf}B_x B_y u+\left[\emptyset\rho_{np}\beta_s+(1-\emptyset)\rho_f\right]g(T-T_c), \quad (3)$$

$$(\rho C_p)_{nf}\left(\frac{\partial T}{\partial t}+u\frac{\partial T}{\partial x}+v\frac{\partial T}{\partial y}\right)=k_{nf}\left(\frac{\partial^2 T}{\partial x^2}+\frac{\partial^2 T}{\partial y^2}\right)+\sigma_{nf}\left(uB_y-vB_x\right)^2-\mu_0 T\frac{\partial M}{\partial T}\left(u\frac{\partial \bar{H}}{\partial x}+v\frac{\partial \bar{H}}{\partial y}\right)+\mu_{nf}\left\{2\left(\frac{\partial u}{\partial x}\right)^2+2\left(\frac{\partial v}{\partial y}\right)^2+\left(\frac{\partial u}{\partial x}+\frac{\partial v}{\partial y}\right)^2\right\}, \quad (4)$$

where ρ, μ, β, α and ϕare the density, the dynamic viscosity, the coefficient of thermal expansion, the thermal diffusivity and the nanoparticles volume fraction, respectively, taking into account s for solid, subscripts f for fluid and nf for nanofluid. In the above equations, the space coordinates, time, velocities and pressure are normalised with the width of the square cylinder h, the characteristic time $\frac{\mathrm{h}}{\mathrm{u_0}}$, the maximum velocity of the channel inlet $\mathrm{u_0}$ and the characteristic pressure $\rho_f\mu_0^2$, respectively. The dimensionless quantities are defined as follows:

$$\theta=\frac{T-T_c}{T_h-T_c},\quad R_e=\frac{\rho_f u_o h}{\mu_f},$$

$$R_i=\frac{Gr}{R_e^2},\ P_r=\frac{v_f}{\alpha_f},$$

$$Gr=\frac{g\beta_f \mathrm{h}(T_h-T_c)}{\mathrm{v_f}^2}$$

$$\tau=\frac{t}{\frac{h}{u_0}},\quad X=\frac{x}{h},\quad Y=\frac{y}{h},\quad U=\frac{u}{u_0},\quad V=\frac{v}{u_0},$$

$$P=\frac{p}{\rho_{nf}u_0^2}$$

$$H_x^*=\frac{H_x}{H_0},\ H_y^*=\frac{H_y}{H_0},\ Mn_f=\frac{\mu_0\,\chi\,H_0^2}{\rho\,u_0^2},$$

$$\mathrm{N}=\frac{\sigma\,\mu_0^2\ H_0^2\,h}{\rho\,u_0^2},\ \mathrm{Ec}=\frac{u_0^2}{C_p\,(T_h-T)}$$

where $\mathrm{T_h}$ and $\mathrm{T_c}$ are hot and cold temperatures, respectively, $\mathrm{v_f}$ is the kinematic viscosity of the base fluid.

Boundary conditions: All solid walls are considered to have no-slip boundary conditions for velocities. The adiabatic properties of both channel walls are described. At the channel inlet, the normal component of velocity is considered to be zero, and the axial velocity is assumed to have a fully formed parabolic profile, given by

$$U=\frac{Y}{4}(4-Y),$$

The convective boundary condition (CBC), at the exit of the channel is given by:

$$\frac{\partial \emptyset}{\partial t}+u_{av}\frac{\partial \emptyset}{\partial X}=0,$$

where the variable φ is the dependent variable (*U, V, θ*). In comparison to the Neumann boundary condition, as described by Sohankar et al. [40] and Abbassi et al. [41], the CBC reduces the number of iterations per time step and requires a smaller upstream computing domain. The square cylinder is considered to be isothermally heated at T_h and exchanging heat with the cold fluid flowing around it, which is at T_c at the channel inlet and is at a uniform temperature.

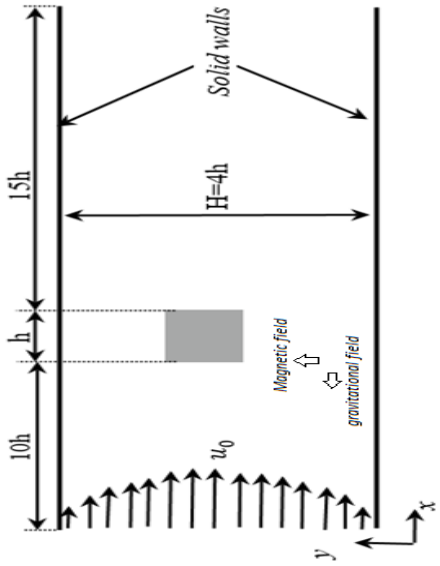

Fig. 1. Physical model of the problem

1.2. Modelling of nanofluids

Based on published relationships, the thermophysical parameters of CuO–water no fluid such as viscosity, density, specific heat and thermal conductivity are estimated.

Viscosity: Masoumi et al. [42] provided a theoretical model based on Brownian motion for predicting the effective viscosity of nanofluids. Their model was demonstrated to effectively predict the effective viscosity of various nanofluids, which is expressed as:

$$\mu_{nf}=\mu_f+\frac{\rho_{np}V_B d_{np}^2}{72C\delta},$$

where

$$V_B=\frac{1}{d_{np}}\sqrt{\frac{18KT}{\pi\rho_{np}d_{np}}},\ \delta=\sqrt[3]{\frac{\pi}{6\varphi}}d_{np}$$

$$C=\mu_f^{-1}\left[\left(c_1 d_{np}\times 10^9+c_2\right)\varphi+\left(c_3 d_{np}\times 10^9+c_4\right)\right],$$

in which

c_1=−0.000001133, c_2=−0.000002771, c_3= 0.00000009, c_4= 0.000000393.

Density: The effective density ρ_{nf} of the nanofluid is expressed as:

$$\rho_{nf}=(1-\phi)\rho_f+\phi\rho_{np}.$$

Specific heat: The following equation, proposed by Xuan and Roetzel [43], is used to compute the specific heat of nanofluids, assuming thermal equilibrium between the base fluid and the nanoparticles:

$$(C_p)_{nf}=\frac{(1-\phi)(\rho C_p)_f+\phi(\rho C_p)_{np}}{(1-\phi)\rho_f+\phi\rho_{np}}$$

The thermal conductivity model established by Koo and Kleinstreuer [36] uses two-term functions to account for the impacts of

particle size d_{np}, particle volumetric concentration φ, temperature T, Brownian motion of nanoparticles and the characteristics of the base fluid. Vajjha and Das [44] improved their model using a larger set of data, as follows:

$$K_{nf} = \frac{(K_{np}+2K_f)-2\phi(K_f-K_{np})}{(K_{np}+2K_f)+\phi(K_f-K_{np})}K_f + 5.10^4\beta\varphi\rho c_{p,f}\sqrt{\frac{kt}{\rho_{nf}d_{np}}}f(T,\varphi)$$

where

$$f(T,\varphi) = (2.8217.10^{-2}\varphi + 3.917.10^{-3})\frac{T}{T_0} + (-3.0669.10^{-2}\varphi - 3.91123.10^{-3})$$

in which, T_0 is set at 273 *K* and the expression of β for CuO nanoparticles is given as follows:

$$\beta = 9.881(100\,\phi)^{-0.9446},$$

which is valid for 298 $K \le T \le$363 K and 1%≤ φ ≤6%.

The values of the nanoparticles and the base fluid properties are required for the thermophysical properties of nanofluid summarised by the preceding equations. In the current work, the CuO nanoparticle characteristics are kept constant in the operating range of 300 K to 350 K, as shown in (Tab. 1):

Tab. 1. Physical Properties of CuO nanoparticles (Dogonchi et al. [45], Abbas et al. [46], Sivaraj et Al. [47])

ρ(kg/m^3)	C_p(J/kg.K)	K(W/mK)	$\beta \times 10^5$(1/K)
6,350	535.6	76.5	1.61

The thermophysical properties of water are considered as a function of the temperature with the following equations (ASHRAE Handbook [48]):

$$\rho_f = -0.0036T^2 + 1.9159T + 748.19,$$

$$c_{p,f} = 0.0001T^3 + 0.1155T^2 - 0.41296T + 0.90178,$$

$$k_f = -8\times10^{-6}T^2 + 0.0062T - 0.5388,\ \mu_f = -0.00002414\times10^{(\frac{247.8}{T-140})}.$$

1.3. Non-dimensional governing equations

The dimensional governing equations will be converted into non-dimensional governing equations with the help of non-dimensional parameters.

$$\frac{\partial U}{\partial X}+\frac{\partial U}{\partial Y} = 0 \quad (5)$$

$$\left(\frac{\partial U}{\partial \tau}+U\frac{\partial U}{\partial X}+V\frac{\partial U}{\partial Y}\right) = -\frac{\partial P}{\partial X}+\frac{\mu_{nf}}{\mu_f}\frac{\rho_f}{\rho_{nf}}\frac{1}{Re}\left(\frac{\partial^2 U}{\partial X^2}+\frac{\partial^2 U}{\partial Y^2}\right)+\frac{\rho_{nf}}{\rho_f}Mn_f H^*\frac{\partial H^*}{\partial X}-\frac{\sigma_{nf}}{\sigma_f}\frac{\rho_f}{\rho_{nf}}N\left(UB_y^{*2}-VB_x^*B_y^*\right) \quad (6)$$

$$\left(\frac{\partial V}{\partial \tau}+U\frac{\partial V}{\partial X}+V\frac{\partial V}{\partial Y}\right) = -\frac{\partial P}{\partial Y}+\frac{\mu_{nf}}{\mu_f}\frac{\rho_f}{\rho_{nf}}\frac{1}{Re}\left(\frac{\partial^2 V}{\partial X^2}+\frac{\partial^2 V}{\partial Y^2}\right)+\frac{\rho_{nf}}{\rho_f}Mn_f H^*\frac{\partial H^*}{\partial Y}-\frac{\sigma_{nf}}{\sigma_f}\frac{\rho_f}{\rho_{nf}}N\left(V\mathrm{B}_x^{*2}-\mathrm{UB}_x^*\mathrm{B}_y^*\right)+Ri\,\frac{\rho_f}{\rho_{nf}}\left(1-\phi+\phi\frac{\rho_{np}}{\rho_f}\frac{\beta_{np}}{\beta_f}\right)\theta \quad (7)$$

$$\left(\frac{\partial \theta}{\partial \tau}+U\frac{\partial \theta}{\partial X}+V\frac{\partial \theta}{\partial Y}\right) = \frac{(\rho C_p)_{nf}}{(\rho C_p)_f}\left[\frac{k_{nf}}{k_f}\frac{1}{Re\,Pr}\left(\frac{\partial^2\theta}{\partial X^2}+\frac{\partial^2\theta}{\partial Y^2}\right)+\frac{\sigma_{nf}}{\sigma_f}N\,Ec\,(U\mathrm{B}_y^*-V\mathrm{B}_x^*)^2-Mn_f\,Ec\,\theta\,H^*\frac{\partial H^*}{\partial\theta}\left(U\frac{\partial H^*}{\partial X}+V\frac{\partial H^*}{\partial Y}\right)+\frac{\mu_{nf}}{\mu_f}\frac{Ec}{Re}\left\{2\left(\frac{\partial U}{\partial X}\right)^2+2\left(\frac{\partial V}{\partial Y}\right)^2+\left(\frac{\partial U}{\partial X}+\frac{\partial V}{\partial Y}\right)^2\right\}\right] \quad (8)$$

1.4. Magnetisation equation

A large external magnetic field has been employed to recirculate flow in dilated regions and increase flow flux into the artery walls. A current plate beneath the bulges generates this magnetisation, which follows the Maxwell's law. The dimensional form of Maxwell's law is given as follows:

$$\nabla\times\bar{H} = J = \sigma(\vec{V}\times \mathrm{B}) \quad (9)$$

$$\nabla.\,\mathrm{B} = \nabla.\,(\mathrm{H}+\mathrm{M}) = 0 \quad (10)$$

also

$$B = \mu_0(M+H),$$

where, μ_0 defines the magnetic permeability of the system, J denotes the electric current density, $\bar{H}$, B represents the magnetic field strength and applied magnetic induction, respectively.

The magnetic field strength and magnetic induction in x & y directions is represented as:

$\bar{H}$= $(\bar{H}_x, \bar{H}_y)$ and $B = (B_x, B_y)$.

The magnetisation process happening in the system is represented by M and it shows the direct relationship with the magnetic field strength.

The mathematical representation of magnetisation is written as follows:

$$M = \chi\ H$$

where χ describes the magnetic susceptibility.

With doing non-dimensional process using non-dimensional parameters, the above equation can be reduced as:

$$\nabla\times H^* = J = \sigma(\overrightarrow{V^*}\times B^*) \quad (11)$$

$$\nabla.\,B^* = \nabla.\,(H^*+M^*) \quad (12)$$

The magnetic field intensity of a current plate is given by:

$$H_y^* = -\frac{H_0}{2}\left[Ln\left(\frac{(x^*-x_2^*)^2+(y^*-y_0^*)^2}{(x^*-x_1^*)^2+(y^*-y_0^*)^2}\right)\right]$$

$$H_x^* = H_0\left[tan^{-1}\left(\frac{(x^*-x_2^*)}{(y^*-y_0^*)}\right)-tan^{-1}\left(\frac{(x^*-x_1^*)}{(y^*-y_0^*)}\right)\right]$$

$$H^* = \sqrt{H_y^{*2}+H_x^{*2}}$$

H_0 is magnetic field strength which depends on applied magnetic induction B, and x_1^*, x_2^*, y_0^* are the position of the horizontal plate. As previously stated, the magnetisation force is created by multiplying the magnetic field and its gradient at various points in space. As a result, the magnetic force near the plate's borders is quite high. This force can alter ferrofluid flow and cause it to deviate from its normal path. The X-component of this force tries to reverse fluid motion, while the Y-component draws particles up-

wards and back into the circulating flow inside the bulges.

The magnetisation property (M*), which is an innate attribute of the ferrofluid, determines the effect of the magnetic field on the flow. This property can be described using a variety of equations, however, in this article, we'll utilise the linear formula [49] that links magnetisation to magnetic field strength and temperature:

$$M^* = \chi_m H^* \tag{13}$$

χ_m is the magnetic susceptibility and varies with temperature:

$$\chi_m = \frac{\chi_0}{1+\beta(T^*-T_0)} \tag{14}$$

χ_0, β and T_0 are constant parameters that are obtained by experimental research.

The applied magnetic induction components in non-dimensional form are written as:

$$\mathrm{B}_x^* = (H_x^* + M^*) = (H_x^* + \chi_m H^*) = \left(H_x^* + \chi_m\sqrt{H_y^{*2} + H_x^{*2}}\right) \tag{15}$$

$$\mathrm{B}_y^* = (H_y^* + M^*) = (H_y^* + \chi_m H^*) = \left(H_y^* + \chi_m\sqrt{H_y^{*2} + H_x^{*2}}\right) \tag{16}$$

1.5. Numerical method of solution

The non-linear governing equations of laminar mixed convection heat transfer in a heated square cylinder with a constant heat flux are solved using ANSYS FLUENT computational fluid dynamics (CFD) coupled with a finite volume approach in a heated square cylinder with constant heat flux. To execute all of the simulations, the ANSYS FLUENT commercial solver was utilised, along with User-Defined Functions that were written to include the effects of magnetic field and represent the MHD-FHD governing equations. A typical scalar transport equation is converted into an algebraic equation that can be solved numerically using the control volume-based technique. It is made up of the following steps:

Using a computational grid, divide the domain into discrete control volumes.

- Integrating the governing equations on individual control volumes to create algebraic equations for discrete dependent variables like velocities, pressure and temperature.
- Linearisation of discretised equations and solution of the resulting linear equation system to produce updated dependent variable values. Details about the solver algorithms used by ANSYS FLUENT can be found in [50].

1.6. Entropy generation

The knowledge of thermodynamics for fluid circulation in confined regions is based on the fundamental idea of entropy generation, which measures the level of disorder within a system.

By taking into account those considerations, a common expression for entropy generation may be formulated as follows [28, 33]:

$$E^{gen} = \frac{k_{nf}\,(\nabla T)}{{T_c}^2} + \frac{\mu_{nf}}{T_c}\left\{2\left(\frac{\partial u}{\partial x}\right)^2 + 2\left(\frac{\partial v}{\partial y}\right)^2 + \left(\frac{\partial u}{\partial x} + \frac{\partial v}{\partial y}\right)^2\right\} + \frac{J^2}{\sigma_{nf}\,T_c} \tag{17}$$

Therefore, the entropy generation expression for fluid flow through a heated square cylinder is

$$E^{gen} = \frac{k_{nf}\left[\left(\frac{\partial T}{\partial x}\right)^2 + \left(\frac{\partial T}{\partial y}\right)^2\right]}{{T_c}^2} + \frac{\mu_{nf}}{T_c}\left\{2\left(\frac{\partial u}{\partial x}\right)^2 + 2\left(\frac{\partial v}{\partial y}\right)^2 + \left(\frac{\partial u}{\partial x} + \frac{\partial v}{\partial y}\right)^2\right\} + \frac{\sigma_{nf}\,(uB_y - vB_x)^2}{T_c} \tag{18}$$

By using Tab. 1, the above dimensional form of entropy generation can be reduced into non-dimensional form, and it will be written as:

$$\bar{E}^{gen} = \frac{E^{gen}}{E}$$

$$\bar{E}^{gen} = \frac{k_{nf}}{k_f}\left[\left(\frac{\partial \theta}{\partial X}\right)^2 + \left(\frac{\partial \theta}{\partial Y}\right)^2\right] + \frac{\mu_{nf}}{\mu_f}\frac{B_r}{AA}\left[2\left(\frac{\partial U}{\partial X}\right)^2 + 2\left(\frac{\partial V}{\partial Y}\right)^2 + \left(\frac{\partial U}{\partial X} + \frac{\partial V}{\partial Y}\right)^2\right] + \frac{\sigma_{nf}}{\sigma_f}\frac{N\,B_r\,Re}{AA}(UB_y^* - VB_x^*)^2 \tag{19}$$

where

$B_r = P_r.E_c$, $\mathrm{AA} = \frac{T_h - T_c}{T_c}$.

1.7. Grid-Independence Analysis

To ensure the stability of numerical simulations, the truncation error becomes negligible when the calculations yield consistent results irrespective of grid density or sparsity. Consequently, the truncation error and the overall validity of numerical outputs hinge on the grid's independence. The reliability of numerical simulations can be significantly impacted by the stability of results with varying grid resolutions. While, in theory, a dense grid could mitigate this concern in grid-independent scenarios, it may lead to unnecessary utilisation of computational resources. Therefore, identifying the optimal grid size is crucial.

Tab. 2. Grid-independence test

Grid	$\frac{k_{nf}}{k_f}$	Nusselt number
100×100	1.154	5.144
200×200	1.125	5.118
400×400	1.1145	5.105
800×800	1.1128	5.085
$1{,}000 \times 1{,}000$	1.1121	5.0846

In the present investigation, determining the optimal grid system involves conducting a 'grid independence test'. This test serves as a mechanism for selecting a mesh density that is both computationally accurate and economically feasible. The optimal grid size, specified as (800×800), is outlined in Tab. 2; further refinement of the mesh size does not enhance accuracy.

2. RESULTS AND DISCUSSION

A complete numerical research employing CuO–water nanofluid and varying magnetic field intensities to analyse laminar mixed convection heat transfer around a heated square cylinder. For various values of magnetic field, Richardson number, volume fraction, size and type (CuO–water) of nanoparticles, numerical simulation results are reported in terms of streamlines, isotherms, velocity magnitude, temperature and average Nusselt number. When compared to some previously published experimental results of CuO–water nanofluids, the current data is found to be similar to Lee et al. [54], implying that they might be used as heat transfer fluids. Tab. 3, provides the default values for different physical parameters and their source of references.

Tab. 3. Range of physical parameters with sources

Parameter	Range	Source
Re	$1-1{,}000$	Uddin et al. [51]
Mn_f	$0-2.02\times10^{12}$	Abdi et al. [52]
N	$0-0.1$	Tzirtzilakis and Xenos [53]
P_r	4.623	Abdi et al. [52]
R_i	$0-10$	Shahi et al. [7]

Figs. 2a and b demonstrate the validation process for the mathematical model formulation and computational method et al. [22], subject to certain assumptions. Specifically, our model disregards the influence of the magnetic field, validation of the Nusselt number is presented graphically, while Fig. 2b illustrates the validation of velocity through nanoparticle absence and the effect of viscous dissipation, while the Newtonian fluid properties have been considered instead of considering non-Newtonian fluid (Power-law fluid) in Bouaziz et al.'s[22] work. The validation process follows accuracy employed in the current research. In Fig. 2a, the contour representation. This validation is conducted by comparing the current research with the findings of Bouaziz the control volume finite element method used in [22], and the simulation of the present work is executed in ANSYS FLUENT Software employing the finite volume methodology. Fig. 2a demonstrates a substantial agreement in Nusselt number between the current study and the observations in [22]. Similarly, Fig. 2b depicts the validation of velocity contours, aligning well with the outcomes of the prior work [22].

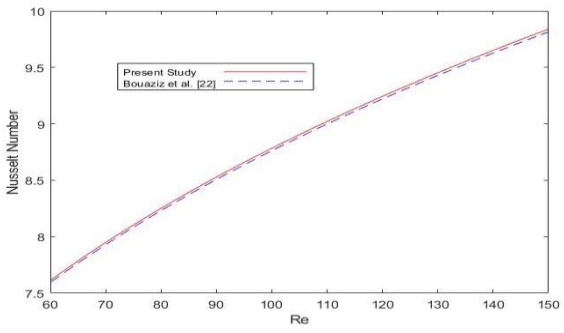

Fig. 2 (a) Validation of Present study for Nusselt number with Bouaziz et al. [22]

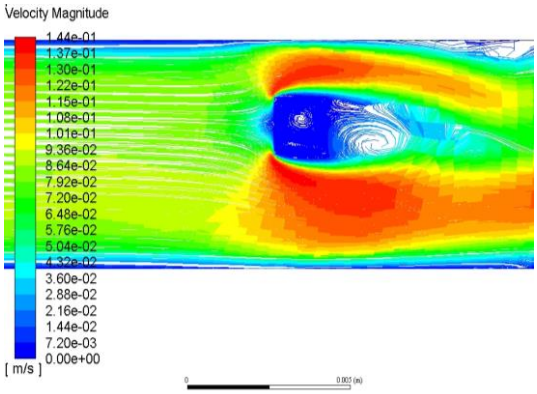

Fig. 2 (b) Contour of velocity magnitude

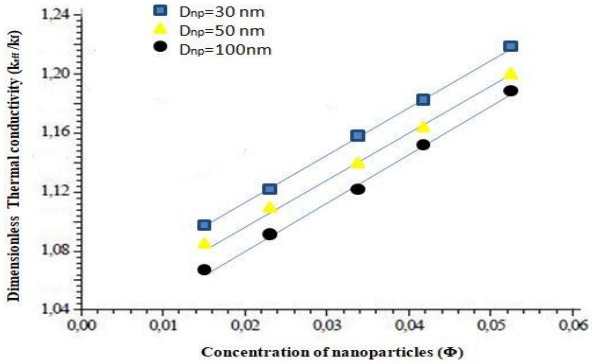

Fig. 3. Thermal conductivity vs concentration of nanoparticles for different values of nanoparticles diameter

Fig. 3 shows the effective thermal conductivity, defined as keff/kf, as a function of particle volume percent and nanoparticle diameter at 300 K. This figure shows that nanoparticles CuO is more thermally conductive than the base fluid water, therefore, when mixed into water, it increases the nanofluid thermal conductivity. Furthermore, as the volume fraction of CuO nanoparticles in the flow increases, the thermal conductivity ratio improves, and this improvement is approximately 12.5% for 0.05 volume fraction when compared to 0.01 volume fraction. This is consistent with other studies, which show that the thermal conductivity of nanofluids rises linearly with particle loading (Philip et al. 55, Shima et al. 56). It is also observed that, for a fixed particle volume fraction, when the smaller diametric size nanoparticles are added into water, it produced more thermal conductivity compared with mixing large diametric nanoparticles. This happens because, small diametric particles quickly dissolve into water and have a higher efficiency of forming strong bonds with water molecules. Therefore, from the figure, it can be easily seen that the thermal conductivity of a particle with a diameter of 30 nm is higher than that of a particle with a diameter of 50 nm or 100 nm.

In Fig. 4, the impact of varied nanoparticle sizes on thermal conductivity (keff/kf) is depicted across different temperatures. It is essential to highlight that as the temperature (T) increases, there is a corresponding increase in thermal conductivity. This phenomenon can be attributed to the incorporation of nanoparticles into the base fluid (water), resulting in an elevation of the fluid's thermal conductivity. Furthermore, the presence of ultra-fine particles induces irregular and chaotic movement within the fluid, thereby enhancing its energy exchange rates [57]. Comparing our findings with previously published experimental results on CuO–water nanofluids, particularly those by Das et al. [58] and Liu et al. [59],

a consistent pattern emerges. The observed similarity suggests robustness and reliability in the behaviour of nanofluids containing different sizes of CuO nanoparticles. Specifically, Fig. 4 elucidates that nanofluids based on water and featuring 30 nm CuO nanoparticles exhibit a significantly higher sensitivity to temperature changes compared to those incorporating particles of sizes 50 nm and 100 nm. This heightened temperature sensitivity underscores the intricate interplay between nanoparticle dimensions and their influence on the thermal properties of the nanofluid system.

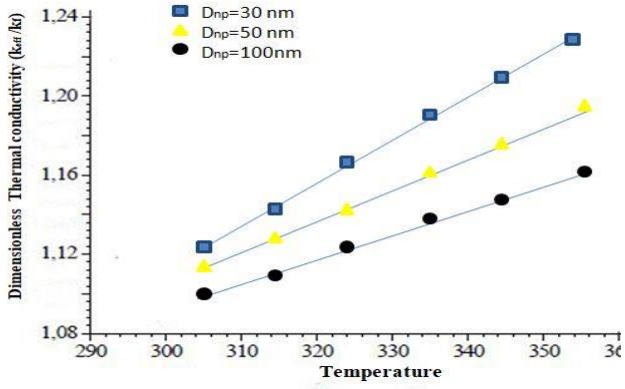

Fig. 4. Thermal conductivity for different values of nanoparticles diameter

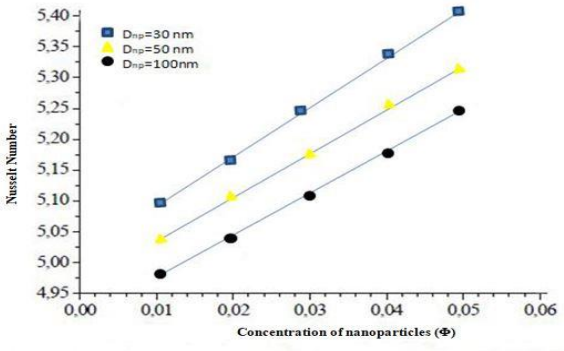

Fig. 5. Nusselt number vs concentration of nanoparticles for different values of nanoparticle diameter

Fig. 5 shows the Nusselt number in relation to nanoparticle concentration for various values of nanoparticle diameter. The heat transfer rate increases monotonically as *dnp* grows for each value of *dnp*, and this enhancement is found to be more substantial for *dnp* = 30 nm than 50 nm and 100 nm. Furthermore, the higher thermal conductivity of the nanofluid is linked to the sensitivity of thermal boundary layer thickness with mass fraction. As a result, higher thermal conductivity values are coupled with higher thermal diffusivity values. As shown, a high degree of thermal diffusivity produces a decrease in temperature gradients and, as a result, an increase in boundary thickness. The Nusselt number is reduced when the thermal boundary layer thickness increases, however, the Nusselt number is a multiplication of the temperature gradient and the heat transfer coefficient. Because the reduction in temperature gradient caused by the presence of nanoparticles is significantly smaller than the thermal conductivity ratio, increasing the bulk fraction improves Nusselt. According to Martnez-Cuencaco et al. [60], the heat transfer improvement achieved in nanofluids is primarily due to a Pr number change (viscosity change). Buschmann [61] also determined that using a combination of Reynolds and Prandtl numbers to describe laminar nanofluid pipe flow with inserted twisted tape is sufficient because two-phase flow effects such as Brownian and thermophoretic diffusion are minor.

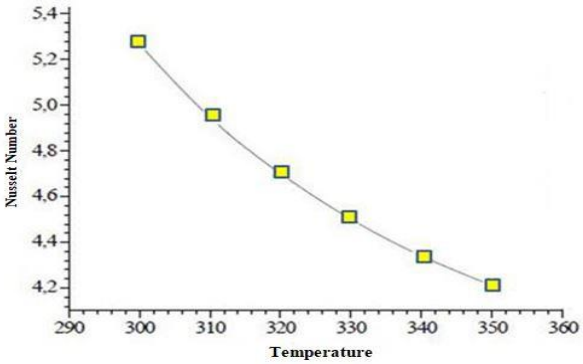

Fig. 6. Nusselt number vs temperature at φ = 5%

In Fig. 6, the variation in global time-averaged Nusselt number under the presence of 5% CuO nanoparticle, is graphically represented in relation to the temperature variable T, specifically over the heat transmission surface of the square cylinder. An interesting phenomenon is visible, in which an increase in temperature T coincides with an observable decrease in heat transfer rate. The diminution in heat transfer with escalating temperature is attributable to a complex interplay of physical factors. One key contributor is the alteration in fluid properties induced by changing temperatures. The transition from T = 300 K to T = 350 K leads to variations in the fluid's viscosity and density, influencing the dynamics of the boundary layer and subsequently affecting the efficiency of convective heat transfer. Additionally, fluctuations in the thermal conductivity of the fluid contribute to its altered capacity for heat conduction. Therefore, a quantified 22% decrease in heat transfer when transitioning from T = 300 K to T = 350 K underscores the system's sensitivity to thermal variations.

Fig. 7 illustrates the fluctuation of the Nusselt number concerning diverse concentrations of nanoparticles under distinct magnetic field strengths. It is evident that the Nusselt number exhibits an upward trend with escalating particle concentration and magnetic field strength. Notably, when the magnetic field intensity is <200 T, the rise in the Nusselt number appears to be more restrained, registering a moderate increase of 6%. However, when the magnetic field strength surpasses 200 T, there is a pronounced and steep ascent in the Nusselt number, reaching an impressive 35%. The observed correlation between increasing particle concentration, magnetic field strength, and the Nusselt number can be elucidated through the underlying physical processes. At lower magnetic field intensities, the response of nanoparticles to the magnetic field is comparatively subdued, resulting in a more controlled enhancement of the Nusselt number. As the magnetic field strength >200 T, the intensified magnetic forces exerted on the nanoparticles lead to a more substantial impact on fluid flow and heat transfer. This heightened influence manifests in a sharp escalation of the Nusselt number, indicating a more pronounced augmentation in convective heat transfer.

Fig. 8 depicts the relationship between the global time-averaged Nusselt Number and the Richardson number for various magnetic field intensities. It is evident that the Nusselt number

DOI 10.2478/ama-2024-0057

falls as the Richardson number rises, whereas the magnetic field has the opposite effect. When the magnetic field strength is increased from 400 T to 500 T, there is a significant difference. The Lorentz force increases as the magnetic field intensity increases, causing a reduction in fluid flow convection in the cylinder and, as a result, an increase in heat transfer across the cylinder as more heat transfer occurs in the system.

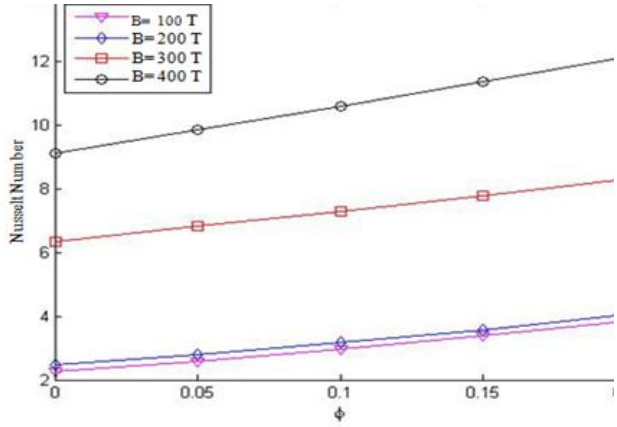

Fig. 7. Nusselt number vs concentration of nanoparticles for different values of magnetic field

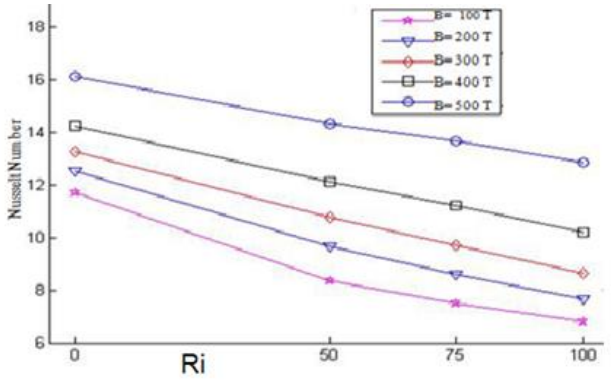

Fig. 8. Nusselt number vs Richardson number for different values of magnetic field

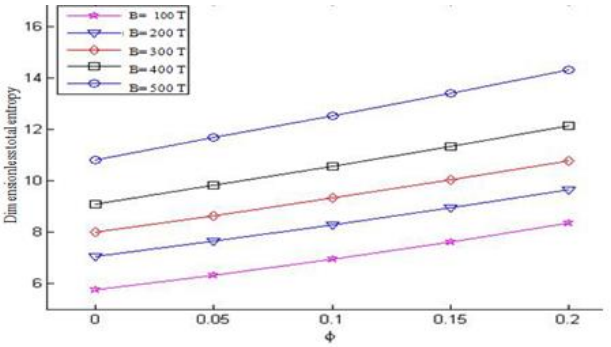

Fig. 9. Entropy for varying intensity of magnetic field

Fig. 9 shows how the dimensionless total entropy changes when the nanoparticle concentration changes at different magnetic strengths. Entropy is basically, the unused energy which further cannot be used for doing mechanical work. The nanoparticles are higher thermal conductive than the water, so when particles are mixed with the water, it enhances the base fluid's thermal conductivity, therefore the temperature of nanofluid enhances significantly according to the volume percentage of nanoparticles. This increased temperature, produces more energy into the flow, but due to sudden surge in energy, most of the energy is not taken for useful works. As a result, the entropy of the flow rises with the mixing of nanoparticles which have more thermal conductivity than the base fluid. Also, it is observed that flow temperature enhances significantly with the increase in magnetic field intensity, due to this, the flow generates more entropy. Therefore, it can be seen through the figure that with the increase in magnetic field intensity, the entropy production into the flow rises significantly.

Contours of static temperature for different sizes of nanofluids are shown in Figs. 10a–c. It is noticed that the contours become less condensed in the region of the top of the cylinder when the size of the nanoparticle decreases. However, when the nanoparticle size increases, the temperature contours are slightly shifted away from the cylinder's surface, resulting in a low-temperature gradient visible from the contours, especially near the rear face, and the thermal boundary layer around the solid walls of the square cylinder is found to be thick. It is obvious from these findings that the nanoparticle dimension dnp = 30 nm has a major impact on the cylinder's stability. Furthermore, the heat transfer rate improves significantly when the size of nanoparticles decreases at the same concentration. Also, the colour range from blue to red represents the temperature variation in the cylinder from minimum to high. It is noted that the length of temperature contours increases when the size of nanoparticle decreases. This is in agreement with the previous study on nanofluids under the influence of magnetic field.

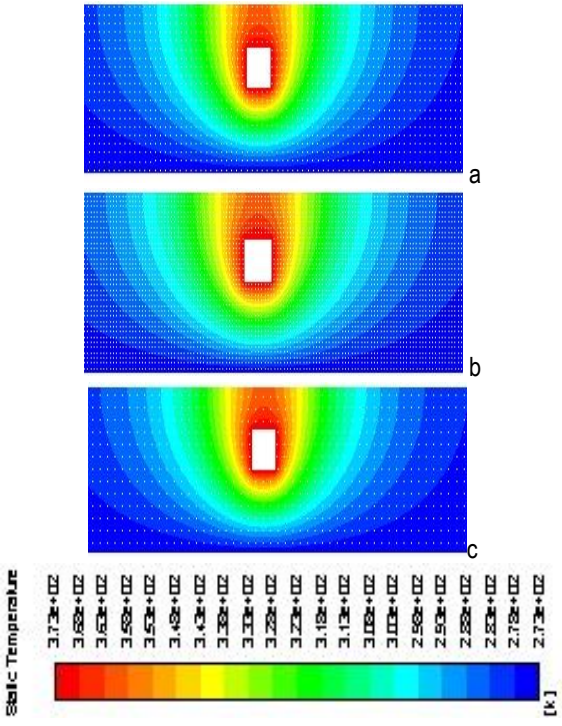

Fig. 10. Contour of total temperature for B = 100 T and dnp = (a) 30 nm (b) 50 nm (c) 80 nm

Figs. 11a–c show the contour of velocity magnitude in the cylinder of CuO–water nanofluid with magnetic field B = 100 T and different sizes of nanoparticles. It can be noted that, for dnp = 50 nm and dnp = 80 nm, the periodic flow is defined by the alternate shedding of vortices into the stream from the bottom face of the

square cylinder. Vortex shedding on both sides of the square cylinder is suppressed at dnp = 30 nm. Vortex shedding is a broad term for a variety of physical phenomena. Vortices are shed alternately from the top and bottom of the cylinder when this happens. The physical changes in the local flow are always followed by the shedding of vortices. It causes pressure and flow velocity to fluctuate in the cylinder's immediate vicinity.

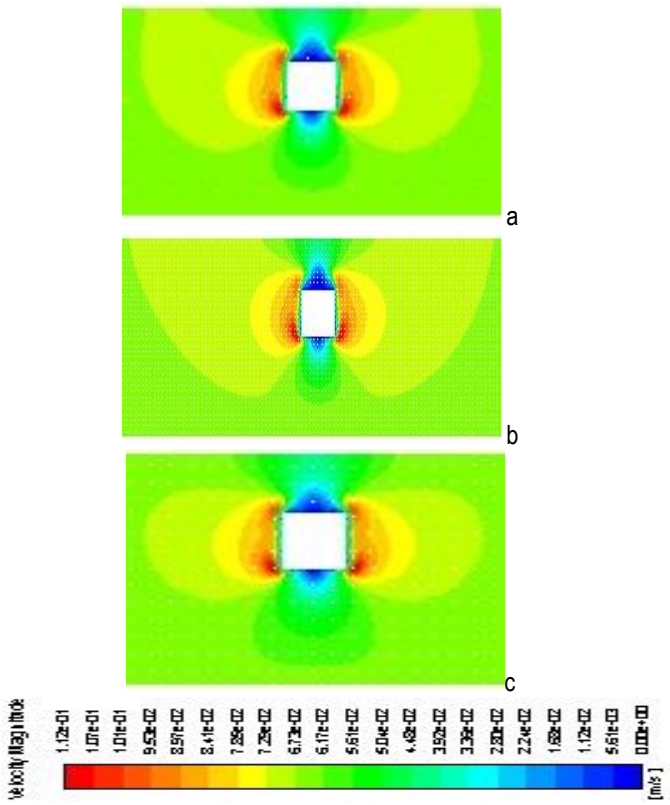

Fig. 11. Contour of velocity magnitude with magnetic field B = 100 T and dnp = (a) 30 nm (b) 50 nm (c) 80 nm

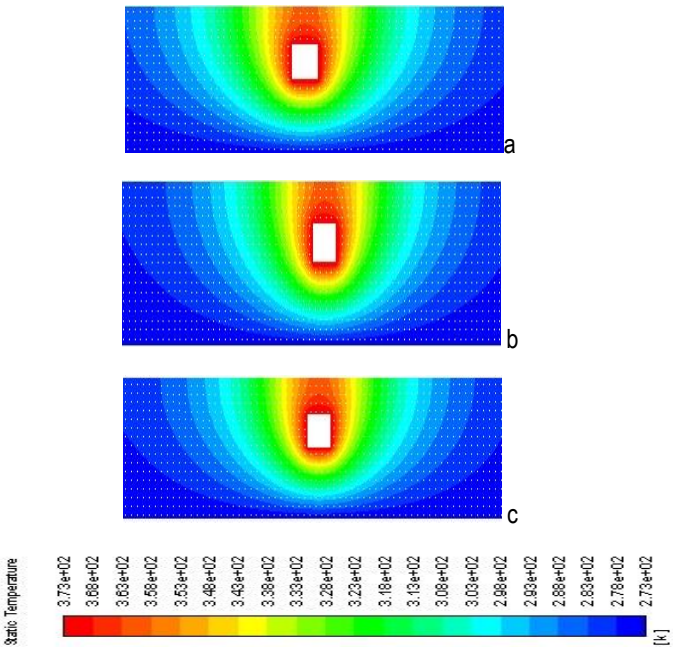

Fig. 12. Contour of static temperature for dnp = 30 nm and magnetic field B (a) 100 T (b) 200 T (c) 300 T

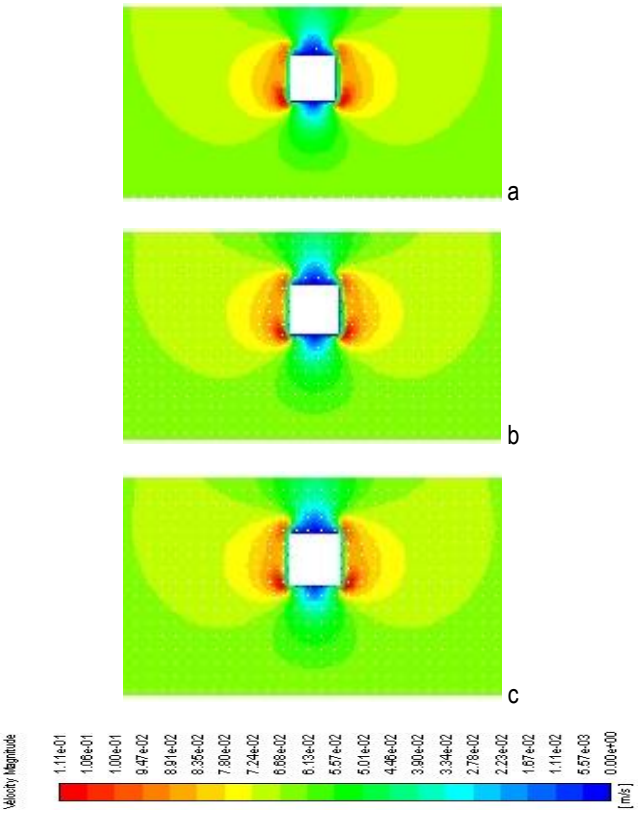

Fig. 13. Contour of velocity magnitude for magnetic field B = (a) 100 T (b) 200 T (c) 300 T

Contours of static temperature for different intensities of magnetic field are shown in Figs. 12a–c. It is observed that the temperature contours are much denser near the front surface of the cylinder, which explains the higher temperature gradient. By increasing the magnetic field strength, the secondary eddy gradually became bigger and the primary eddy became smaller. The isotherms show that the effect of the magnetic field is suppressing the convective heat transfer mechanism. This is due to uniformly distributed isotherms in the cavity, especially at the bottom. It is also clear that the heat transfer curve reaches a peak at the corners of the top and bottom surfaces of the cylinder which is due to the high temperature gradients at these points.

Contours of velocity magnitude for dnp = 30 nm in the cylinder with different intensities of magnetic fields are shown in Fig. 13a–c. When the intensity of the magnetic field drops, the length of the velocity contours increases. This means that the magnetic field causes the fluid flow to slow down, resulting in higher heat transfer in the system. As a result of the increased magnetic field, the heat transfer across the cylinder increases, and the velocity of the CuO–water nanofluid drops. The Lorentz force increases as the magnetic field strength increases, resulting in less fluid flow convection in the cylinder, as evidenced by the decrease in vortexes as the magnetic field intensity rises.

Fig. 14 depicts the streamlines of the fluid crossing the square cylinder in the channel at various intensities of the applied magnetic field (a–c). With a rise in the magnetic field, the heat convection across the cylinder increases but the velocity falls marginally. The periodic flow defined by the alternate shedding of vortices from the bottom face of the square cylinder into the stream may be seen for B = 200 T and B = 300 T. Vortex shedding is suppressed at the top of the square cylinder when B = 100 T.

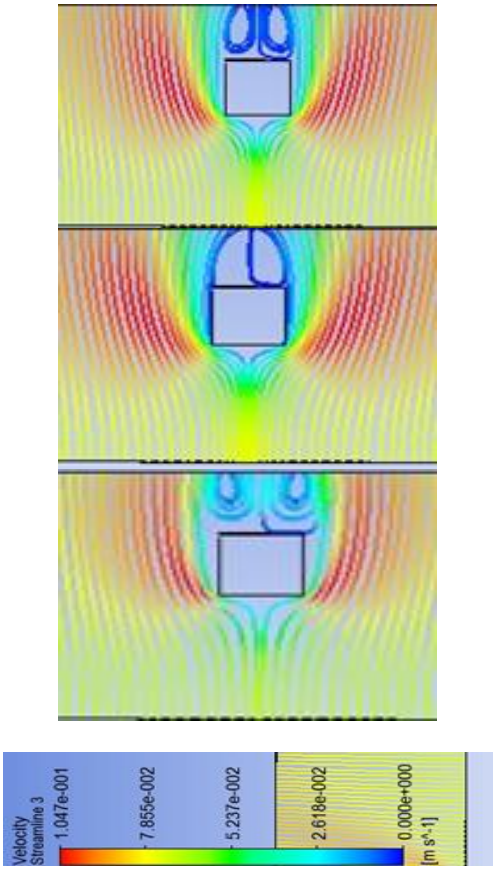

Fig. 14. Streamlines Velocity in the cylinder with dnp = 30 nm and the influence of magnetic field B (a) 100 T (b) 200 T (c) 300 T

3. CONCLUSIONS

A numerical analysis of unsteady, laminar flow and heat transfer of CuO–water nanofluid past a heated square cylinder inside a vertical channel has been discussed in the presence of a magnetic field. The entropy generation also calculates different magnetic field intensities for various nanoparticle volume fractions. In this work, the impact of several parameters such as nanoparticle volume fraction, nanoparticle size, magnetic field intensity, Richardson number on the velocity, thermal conductivity, Nusselt number and entropy profile have been discussed with the help of both graphs and contours. This computational study is performed using the ANSYS FLUENT CFD software, which uses the finite volume approach for solving governing equations. The findings are poised to influence the design and optimisation of various technological applications, spanning electronic devices, cooling systems and other engineering domains where efficient heat transfer is paramount. Thus, the research not only expands the current scientific understanding but also directly informs and advances technology with real-world applications. The following is the conclusion reached as a result of this research:

- As the Richardson number rises, it induces a reduction in the Nusselt number, while conversely, the intensity of the magnetic field exerts a contrasting influence, leading to an augmentation in its effect.
- Diminishing the nanoparticle size results in an elevation of the Nusselt number at a specified concentration, whereas amplifying the nanoparticle concentration leads to an increased Nusselt number at a given particle size.
- The incorporation of nanoparticles improves thermal conductivity and alters the structure of the flow field, consequently leading to heightened heat transfer.
- The stability of the cylinder is notably influenced by the nanoparticle diameter, specifically when the diameter is observed to be *dnp* = 30 nm.
- The entropy of a flow is directly related to nanoparticle volume fraction and magnetic field intensity.

List of Symbols:

C_p= specific heat of the fluid
H = channel width
d = diameter
h = side length of a square cylinder
t = time
k = thermal conductivity
L = length of the channel
P_r = Prandtl number
R_i = Richardson number
T = dimensional temperature
t = time nondimensionalised by u_0/h
u_o= mean cHannel inlet velocity
V = velocity vector numdimensionalised by U_o
X_u= distance from body to inlet
X_d= distance from body to outlet
μ_f= base fluid viscocity
μ_{nf}= nanofluid viscocity
K_s= thermal conductivity of metallic nanoparticle
K_f= thermal conductivity of base fluid
K_{nf}= thermal conductivity of nanofluid
ρ_s= metallic nanoparticle density
ρ_f= base fluid density
ρ_{nf}= nanofluid density
$(\rho C_p)_f$= heat capacitance of base fluid
$(\rho C_p)_{nf}$= heat capacitance of nanofluid
$(\rho\gamma)_{nf}$= thermal expansion coefficient of nanofluid
Φ = volume fraction
G_r= Grashof number
R_e= Reynolds number
B_r= Brinkman number
E_c= Eckert number
E^{gen} = entropy generation
B_{np}= coefficient of thermal expansion
B_x= x-component of the magnetic flux density
B_y= y-component of the magnetic flux density

REFERENCES

1. Seyyedi SM, Hashemi-Tilehnoee M, del Barrio EP, Dogonchi AS, Sharifpur M. Analysis of magneto-natural-convection flow in a semi-annulus enclosure filled with a micropolar-nanofluid; a computational framework using CVFEM and FVM. Journal of Magnetism and Magnetic Materials. 2023; 568:170407. https://doi.org/10.1016/j.jmmm.2023.170407
2. Abbas N, Nadeem S, Issakhov A. Transportation of modified nanofluid flow with time dependent viscosity over a Riga plate: exponentially stretching. Ain Shams Engineering Journal. 2021;12(4):3967-73. https://doi.org/10.1016/j.asej.2021.01.034
3. Lee S, Choi SS, Li SA, Eastman JA. Measuring thermal conductivity of fluids containing oxide nanoparticles. 1999;121:280–289. https://doi.org/10.1115/1.2825978
4. Mostafizur RM, Saidur R, Aziz AA, Bhuiyan MH. Thermophysical properties of methanol based Al2O3 nanofluids. International Journal of Heat and Mass Transfer. 2015;85:414-9. https://doi.org/10.1016/j.ijheatmasstransfer.2015.01.075

5. Sharma BK, Kumawat C, Bhatti MM. Optimizing energy generation in power-law nanofluid flow through curved arteries with gold nanoparticles. Numerical Heat Transfer, Part A: Applications. 2023;1-33. https://doi.org/10.1080/10407782.2023.2232123
6. Wen D, Ding Y. Experimental investigation into convective heat transfer of nanofluids at the entrance region under laminar flow conditions. International journal of heat and mass transfer. 2004;47(24):5181-8. https://doi.org/10.1016/ j.ijheatmasstransfer.2004.07.012
7. Shahi M, Mahmoudi AH, Talebi F. Numerical study of mixed convective cooling in a square cavity ventilated and partially heated from the below utilizing nanofluid. International Communications in Heat and Mass Transfer. 2010;37(2):201-13. https://doi.org/10.1016/j.icheatmasstransfer.2009.10.002
8. Bovand M, Rashidi S, Esfahani JA. Enhancement of heat transfer by nanofluids and orientations of the equilateral triangular obstacle. Energy conversion and management. 2015;97:212-23. https://doi.org/10.1016/j.enconman.2015.03.042
9. Hayat T, Khan MI, Waqas M, Alsaedi A, Farooq M. Numerical simulation for melting heat transfer and radiation effects in stagnation point flow of carbon–water nanofluid. Computer methods in applied mechanics and engineering. 2017;315:1011-24. https://doi.org/10.1016/j.cma.2016.11.033
10. Hayat T, Waqas M, Alsaedi A, Bashir G, Alzahrani F. Magnetohydrodynamic (MHD) stretched flow of tangent hyperbolic nanoliquid with variable thickness. Journal of molecular liquids. 2017 Mar 1;229:178-84. Available from : https://doi.org/10.1016/j.molliq.2016.12.058
11. Sheikholeslami M, Ellahi R. Electrohydrodynamic nanofluid hydrothermal treatment in an enclosure with sinusoidal upper wall. Applied Sciences. 2015;5(3):294-306. https://doi.org/10.3390/app5030294
12. Sheikholelami M, Chamkha AJ. Electrohydrodynamic free convection heat transfer of a nanofluid in a semi-annulus enclosure with a sinusoidal wall. Numerical Heat Transfer, Part A: Applications. 2016;69(7):781-93. https://doi.org/10.1080/10407782.2015.1090819
13. Kandelousi MS, Ellahi R. Simulation of ferrofluid flow for magnetic drug targeting using the lattice Boltzmann method. Zeitschrift für Naturforschung A. 2015;70(2):115-24. https://doi.org/10.1515/zna-2014-0258
14. Sarfraz M, Khan M, Al-Zubaidi A, Saleem S. Tribology-informed analysis of convective energy transfer in ternary hybrid nanofluids on inclined porous surfaces. Tribology International. 2023;188:108860. https://doi.org/10.1016/j.triboint.2023.108860
15. Sarfraz M, Khan M, Al-Zubaidi A, Saleem S. Enhancing energy transport in Homann stagnation-point flow over a spiraling disk with ternary hybrid nanofluids. Case Studies in Thermal Engineering. 2023;49:103134. https://doi.org/10.1016/j.csite.2023.103134
16. Chaudhary RC, Sharma BK. Combined heat and mass transfer by laminar mixed convection flow from a vertical surface with induced magnetic field. Journal of Applied Physics. 2006;99(3):034901. https://doi.org/10.1063/1.2161817
17. Sharma BK, Mishra A, Gupta S. Heat and mass transfer in magneto-biofluid flow through a non-Darcian porous medium with Joule effect. Journal of Engineering Physics and Thermophysics. 2013;86:766-74.
17. https://link.springer.com/article/10.1007/s10891-013-0893-0
18. Raj Kumawat S, Vyas H, Mohan R, Sasidharan R, Yadav B, Gupta N. 90 versus 60 min of early skin-to-skin contact on exclusive breastfeeding rate in healthy infants'≥ 35 weeks: A randomised controlled trial. Acta Paediatrica. 2024;113(2):199-205. https://doi.org/10.1111/apa.17021
19. Mishra A, Sharma BK. MHD mixed convection flow in a rotating channel in the presence of an inclined magnetic field with the Hall effect. Journal of Engineering Physics and Thermophysics. 2017; 90:1488-99. https://doi.org/10.1007/s10891-017-1710-y
20. Sharma S, Maiti DK, Alam MM, Sharma BK. Nanofluid flow and heat transfer from heated square cylinder in the presence of upstream rectangular cylinder under Couette-Poiseuille flow. Wind Struct. 2019;29(1):65-75. https://doi.org/10.12989/was.2019.29.1.065
21. Turki S, Abbassi H, Nasrallah SB. Effect of the blockage ratio on the flow in a channel with a built-in square cylinder. Computational Mechanics. 2003;33:22-9. https://doi.org/10.1007/s00466-003-0496-2
22. Bouaziz M, Kessentini S, Turki S. Numerical prediction of flow and heat transfer of power-law fluids in a plane channel with a built-in heated square cylinder. International Journal of Heat and Mass Transfer. 2010;53(23-24):5420-9. https://doi.org/10.1016/j.ijheatmasstransfer.2010.07.014
23. Hayat T, Anwar MS, Farooq M, Alsaedi A. Mixed convection flow of viscoelastic fluid by a stretching cylinder with heat transfer. Plos one. 2015;10(3):e0118815. https://doi.org/10.1371/journal.pone.0118815
24. Sharma BK, Sharma P, Mishra NK, Fernandez-Gamiz U. Darcy-Forchheimer hybrid nanofluid flow over the rotating Riga disk in the presence of chemical reaction: artificial neural network approach. Alexandria Engineering Journal. 2023;76:101-30. https://doi.org/10.1016/j.aej.2023.06.014
25. Kumar A, Sharma BK, Gandhi R, Mishra NK, Bhatti MM. Response surface optimization for the electromagnetohydrodynamic Cu-polyvinyl alcohol/water Jeffrey nanofluid flow with an exponential heat source. Journal of Magnetism and Magnetic Materials. 2023;576:170751. https://doi.org/10.1016/j.jmmm.2023.170751
26. Sharma BK, Sharma P, Mishra NK, Noeiaghdam S, Fernandez-Gamiz U. Bayesian regularization networks for micropolar ternary hybrid nanofluid flow of blood with homogeneous and heterogeneous reactions: Entropy generation optimization. Alexandria Engineering Journal. 2023;77:127-48. https://doi.org/10.1016/j.aej.2023.06.080
27. Sharma BK, Khanduri U, Mishra NK, Chamkha AJ. Analysis of Arrhenius activation energy on magnetohydrodynamic gyrotactic microorganism flow through porous medium over an inclined stretching sheet with thermophoresis and Brownian motion. Proceedings of the Institution of Mechanical Engineers, Part E: Journal of Process Mechanical Engineering. 2023;237(5):1900-14. https://doi.org/10.1177/09544089221128768
28. Dogonchi AS, Mishra SR, Chamkha AJ, Ghodrat M, Elmasry Y, Alhumade H. Thermal and entropy analyses on buoyancy-driven flow of nanofluid inside a porous enclosure with two square cylinders: Finite element method. Case Studies in Thermal Engineering. 2021;27:101298. https://doi.org/10.1016/j.csite.2021.101298
29. Afshar SR, Mishra SR, Dogonchi AS, Karimi N, Chamkha AJ, Abulkhair H. Dissection of entropy production for the free convection of NEPCMs-filled porous wavy enclosure subject to volumetric heat source/sink. Journal of the Taiwan Institute of Chemical Engineers. 2021;128:98-113. https://doi.org/10.1016/j.jtice.2021.09.006
30. Shao W, Nayak MK, El-Sapa S, Chamkha AJ, Shah NA, Galal AM. Entropy optimization of non-Newtonian nanofluid natural convection in an inclined U-shaped domain with a hot tree-like baffle inside and considering exothermic reaction. Journal of the Taiwan Institute of Chemical Engineers. 2023;148:104990. https://doi.org/10.1016/j.jtice.2023.104990
31. Dogonchi AS, Bondareva NS, Sheremet MA, El-Sapa S, Chamkha AJ, Shah NA. Entropy generation and heat transfer performance analysis of a non-Newtonian NEPCM in an inclined chamber with complicated heater inside. Journal of Energy Storage. 2023;72:108745. https://doi.org/10.1016/j.est.2023.108745
32. Nayak MK, Dogonchi AS, Rahbari A. Free convection of Al2O3-water nanofluid inside a hexagonal-shaped enclosure with cold diamond-shaped obstacles and periodic magnetic field. Case Studies in Thermal Engineering. 2023;50:103429. https://doi.org/10.1016/j.csite.2023.103429
33. Sharma BK, Kumawat C, Makinde OD. Hemodynamical analysis of MHD two phase blood flow through a curved permeable artery having variable viscosity with heat and mass transfer. Biomechanics and Modeling in Mechanobiology. 2022;21(3):797-825. https://doi.org/10.1007/s10237-022-01561-w

34. Sharma BK, Kumawat C, Khanduri U, Mekheimer KS. Numerical investigation of the entropy generation analysis for radiative mhd power-law fluid flow of blood through a curved artery with hall effect. Waves in Random and Complex Media. 2023:1-38. https://doi.org/10.1080/17455030.2023.2226228
35. Kumawat C, Sharma BK, Al-Mdallal QM, Rahimi-Gorji M. Entropy generation for MHD two phase blood flow through a curved permeable artery having variable viscosity with heat and mass transfer. International Communications in Heat and Mass Transfer. 2022;133: 105954. https://doi.org/10.1016/j.icheatmasstransfer.2022.105954
36. Koo J, Kleinstreuer C. Laminar nanofluid flow in microheat-sinks. International journal of heat and mass transfer. 2005;48(13):2652-61. https://doi.org/10.1016/j.ijheatmasstransfer.2005.01.029
37. Santra AK, Sen S, Chakraborty N. Study of heat transfer due to laminar flow of copper–water nanofluid through two isothermally heated parallel plates. International journal of thermal sciences. 2009;48(2):391-400.https://doi.org/10.1016/j.ijthermalsci.2008.10.004
38. Yasmeen T, Hayat T, Khan MI, Imtiaz M, Alsaedi A. Ferrofluid flow by a stretched surface in the presence of magnetic dipole and homogeneous-heterogeneous reactions. Journal of Molecular liquids. 2016;223:1000-5. https://doi.org/10.1016/j.molliq.2016.09.028
39. Nawaz M, Nazir U, Saleem S, Alharbi SO. An enhancement of thermal performance of ethylene glycol by nano and hybrid nanoparticles. Physica A: Statistical Mechanics and its Applications. 2020;551:124527. https://doi.org/10.1016/j.physa.2020.124527
40. Sohankar A, Norberg C, Davidson L. Low-Reynolds-number flow around a square cylinder at incidence: study of blockage, onset of vortex shedding and outlet boundary condition. International journal for numerical methods in fluids. 1998;26(1):39-56. https://doi.org/10.1002/(SICI)1097-0363
41. Abbassi H, Turki S, Nasrallah SB. Channel flow past bluff-body: outlet boundary condition, vortex shedding and effects of buoyancy. Computational Mechanics.2002;28(1):10-6. https://doi.org/10.1007/s004660100261
42. Masoumi N, Sohrabi N, Behzadmehr A. A new model for calculating the effective viscosity of nanofluids. Journal of Physics D: Applied Physics. 2009;42(5):055501. DOI 10.1088/0022-3727/42/5/055501
43. Xuan Y, Roetzel W. Conceptions for heat transfer correlation of nanofluids. International Journal of heat and Mass transfer. 2000;43(19):3701-7. https://doi.org/10.1016/S0017-9310(99)00369-5
44. Vajjha RS, Das DK. Experimental determination of thermal conductivity of three nanofluids and development of new correlations. International journal of heat and mass transfer. 2009;52(21-22):4675-82. https://doi.org/10.1016/j.ijheatmasstransfer.2009.06.027
45. Dogonchi AS, Waqas M, Afshar SR, Seyyedi SM, Hashemi-Tilehnoee M, Chamkha AJ, Ganji DD. Investigation of magneto-hydrodynamic fluid squeezed between two parallel disks by considering Joule heating, thermal radiation, and adding different nanoparticles. International Journal of Numerical Methods for Heat & Fluid Flow. 2020;30(2):659-80. https://doi.org/10.1108/HFF-05-2019-0390
46. Abbas N, Nadeem S, Issakhov A. Transportation of modified nanofluid flow with time dependent viscosity over a Riga plate: exponentially stretching. Ain Shams Engineering Journal. 2021;12(4):3967-73. https://doi.org/10.1016/j.asej.2021.01.034
47. Sivaraj R, Animasaun IL, Olabiyi AS, Saleem S, Sandeep N. Gyrotactic microorganisms and thermoelectric effects on the dynamics of 29 nm CuO-water nanofluid over an upper horizontal surface of paraboloid of revolution. Multidiscipline Modeling in Materials and Structures. 2018 Oct 8;14(4):695-721. https://doi.org/10.1108/MMMS-10-2017-0116
48. Owen MS. ASHRAE Handbook: Fundamentals, American Society of Heating. Refrigeration and Air-Conditioning Engineers. 2009.
49. Scarpa F, Smith FC. Passive and MR fluid-coated auxetic PU foam–mechanical, acoustic, and electromagnetic properties. Journal of intelligent material systems and structures. 2004;15(12):973-9. https://doi.org/10.1177/1045389X04046610
50. ANSYS C. Reference Guide. Release 12.1. ANSYS. Inc. 2009.
51. Uddin MJ, Rasel SK, Rahman MM, Vajravelu K. Natural convective heat transfer in a nanofluid-filled square vessel having a wavy upper surface in the presence of a magnetic field. Thermal Science and Engineering Progress. 2020;19:100660. https://doi.org/10.1016/j.tsep.2020.100660
52. Abdi H, Motlagh SY, Soltanipour H. Study of magnetic nanofluid flow in a square cavity under the magnetic field of a wire carrying the electric current in turbulence regime. Results in Physics. 2020;18:103224. https://doi.org/10.1016/j.rinp.2020.103224
53. Tzirtzilakis EE, Xenos MA. Biomagnetic fluid flow in a driven cavity. Meccanica. 2013;48:187-200. https://doi.org/10.1007/s11012-012-9593-7
54. Lee S, Choi SS, Li SA, Eastman JA. Measuring thermal conductivity of fluids containing oxide nanoparticles.1999;121(2): 280-289. https://doi.org/10.1115/1.2825978
55. Philip J, Shima PD, Raj B. Evidence for enhanced thermal conduction through percolating structures in nanofluids. Nanotechnology. 2008;19(30):305706. DOI 10.1088/0957-4484/19/30/305706
56. Shima PD, Philip J, Raj B. Influence of aggregation on thermal conductivity in stable and unstable nanofluids. Applied Physics Letters. 2010;97(15). https://doi.org/10.1063/1.3497280
57. Xuan Y, Li Q. Heat transfer enhancement of nanofluids. International Journal of heat and fluid flow. 2000;21(1):58-64. https://doi.org/10.1016/S0142-727X(99)00067-3
58. Das SK, Putra N, Thiesen P, Roetzel W. Temperature dependence of thermal conductivity enhancement for nanofluids. J. Heat Transfer. 2003;125(4):567-74. https://doi.org/10.1115/1.1571080
59. Liu MS, Lin MC, Huang IT, Wang CC. Enhancement of thermal conductivity with CuO for nanofluids. Chemical Engineering & Technology: Industrial Chemistry-Plant Equipment-Process Engineering-Biotechnology. 2006;29(1):72-7. https://doi.org/10.1002/ceat.200500184
60. Martínez-Cuenca R, Mondragón R, Hernández L, Segarra C, Jarque JC, Hibiki T, Juliá JE. Forced-convective heat-transfer coefficient and pressure drop of water-based nanofluids in a horizontal pipe. Applied Thermal Engineering. 2016;98:841-9. https://doi.org/10.1016/j.applthermaleng.2015.11.050
61. Buschmann MH. Nanofluid heat transfer in laminar pipe flow with twisted tape. Heat Transfer Engineering. 2017;38(2):162-76. https://doi.org/10.1080/01457632.2016.1177381

The authors would like to express sincere gratitude to Al Maarefa University, Riyadh, Saudi Arabia for supporting this research.

Madhu Sharma: https://orcid.org/0000-0002-9154-6708
Bhupendra K. Sharma: https://orcid.org/0000-0002-2051-9681
Chandan Kumawat: https://orcid.org/0000-0002-3366-2807
Arun K. Jalan: https://orcid.org/0000-0001-5382-1521
Neyara Radwan: https://orcid.org/0000-0001-8756-4834